Conformation Coupled Enzyme Catalysis: Single-Molecule and Transient Kinetics Investigation of Dihydrofolate Reductase†

Nina M. Antikainen,‡ R. Derike Smiley,§ Stephen J. Benkovic,‡ and Gordon G. Hammes*,§

Department of Chemistry, Pennsylvania State University, 152 Davey Laboratory, University Park, Pennsylvania 16802, and Department of Biochemistry, Duke University Medical Center, P.O. Box 3711, Durham, North Carolina 27710

Received July 15, 2005; Revised Manuscript Received September 21, 2005

ABSTRACT: Ensemble kinetics and single-molecule fluorescence microscopy were used to study conformational transitions associated with enzyme catalysis by dihydrofolate reductase (DHFR). The active site loop of DHFR was labeled with a fluorescence quencher, QSY35, at amino acid position 17, and the fluorescent probe, Alexa555, at amino acid 37, by introducing cysteines at these sites with site-specific mutagenesis. The distance between the probes was such that approximately 50% fluorescence resonance energy transfer (FRET) occurred. The double-labeled enzyme retained essentially full catalytic activity, and stopped-flow studies of both the forward and reverse reactions revealed that the distance between probes increased prior to hydride transfer. A fluctuation in fluorescence intensity of single molecules of DHFR was observed in an equilibrium mixture of substrates but not in their absence. Ensemble rate constants were derived from the distributions of lifetimes observed and attributed to a reversible conformational change. Studies were carried out with both NADPH and NADPD as substrates, with no measurable isotope effect. Similar studies with a G121V mutant DHFR resulted in smaller rate constants. This mutant DHFR has reduced catalytic activity, so that the collective data for the conformational change suggest that the conformational change being observed is associated with catalysis and probably represents a conformational change prior to hydride transfer. If the change in fluorescence is attributed to a change in FRET, the distance change associated with the conformational change is approximately 1−2 Å. These results are correlated with other measurements related to conformation coupled catalysis.

Dihydrofolate reductase (DHFR)[1] catalyzes the reduction of dihydrofolate by NADPH to tetrahydrofolate and $NADP^+$. The enzyme is of physiological importance in the biosynthesis of purines, thymidylate, and a number of amino acids, and its strategic location in metabolism has made it a target for anticancer drugs such as methotrexate and the antibacterial agent trimethoprim. The mechanism of action and molecular structure of DHFR from *Escherichia coli* have been extensively studied so that it also has become a paradigm for attempting to understand the fundamental nature of enzyme catalysis (cf. *1*−*4*).

The mechanism of action of DHFR involves multiple conformational changes that include domain rotations and the movement of structural loops (cf. *1*, *4*). The dynamics of the enzyme mechanism have been probed with steady state, transient, and single-molecule kinetics (cf. *2*−*6*). Although conformational transitions have been clearly established as an important element in enzyme catalysis, their precise role is still a matter of speculation (cf. *7*−*12*). Among the open questions is whether the conformational changes play a dynamic or static role; that is, do the conformational changes simply establish a favorable environment for specific catalytic steps to occur and/or do they actually participate in catalysis in a more dynamic way. Also, do the conformational changes involve only residues near the active site, or is the entire molecule involved? In the case of DHFR, it has been shown that the environment of residues distant from the catalytic site is altered during catalysis (*4*, *13*), and theoretical calculations suggest that significant movements of residues occur as the hydride transfer takes place (*14*).

In this work, single-molecule and transient kinetics have been used to probe the coordination of conformational changes with catalysis and the magnitude of the conformational changes that occur. This has been accomplished by constructing a mutant of *E. coli* DHFR (molecular weight ∼ 20 000) with cysteine residues only at positions 17 and 37. Residue 17 is part of a structural loop that closes over the active site during catalysis, whereas residue 37 is not near the active site. Residue 37 is located in the hinge region that connects the αB and βB sheets in a pivot point for movement between two DHFR substructures, the major domain and the adenosine binding domain (*15*). Both cysteines are readily accessible to solvent, and the side chains are not involved in significant interactions with other DHFR residues in any of the known DHFR conformations. The structure of DHFR is shown in Figure 1, with the positions of residues 17 and 37 indicated. Subsequently, residues 17 and 37 were labeled with the fluorescence acceptor QSY35

† Supported by National Institutes of Health Grants GM 65128 (G.G.H.) and GM 24129 (S.J.B.).

* Corresponding author. Phone, (919) 684-8848; fax, (919)684-9709; e-mail, hamme001@mc.duke.edu.

‡ Pennsylvania State University.

§ Duke University Medical Center.

[1] Abbreviations: Alexa555, Alexa fluor 555 dye; Alexa488, Alexa fluor 488 dye; DHFR, dihydrofolate reductase; DHF, dihydrofolate; FRET, fluorescence resonance energy transfer.

10.1021/bi051378i CCC: $30.25
Published on Web 12/03/2005

FIGURE 1: Structure of *E. coli* DHFR with bound $NADP^+$ (green) and folic acid (purple; PDB 1rx2). Amino acids 17 and 37 are shown as yellow spheres, indicating the location of the QSY35 and Alexa555 (purple and orange stars, respectively). Residue 121 is shown as a lime green sphere.

and the fluorescent probe Alexa555. The distance between these two probes when attached to DHFR residues 17 and 37 is estimated as 22−31 Å from the known structures, and the distance at which 50% fluorescence resonance energy transfer (FRET) occurs, R_0, is 24 Å. Thus, about 50% FRET is expected to occur.

The fluorescence of Alexa555 was monitored to study conformational changes associated with hydride transfer. The changes in FRET, in principle, are a measure of distance changes between the two probes associated with these reactions. The results obtained from ensemble and single-molecule studies suggest that the DHFR-catalyzed reaction is associated with conformational changes in both the forward and reverse reactions and also provide an approximate measure of the extent of the associated conformational changes.

MATERIALS AND METHODS

Preparation of Mutant Biotinylated DHFR. The preparation of DHFR with a cysteine only at amino acid position 17 and a biotinylation signal sequence (bioseq) at the N-terminus has been described previously (*16*). To label DHFR selectively at position 17, native cysteines were removed from DHFR by using a gene that codes for the replacements C85A and C152S (ΔCys) as previously described (*16*). Residues 85 and 152 are located in helix αE in the adenosine binding domain and sheet βH in the major domain, respectively. The enzyme with these replacements has comparable binding and catalytic properties to wild-type DHFR. A construct with a cysteine also at amino acid position 37 for double-labeling purposes was prepared from the bioseq-ΔCys-E17C-DHFR pET27b plasmid. The plasmid was amplified by overlap extension PCR protocols utilizing mutagenic internal primers 5′-GTGCCCAAATGTATTC-CACAAC-3′ (forward) and 5′-GTTGTGGAATACATTTG-GCAC-3′ (reverse) and the nonmutagenic external T7 and T7rev primers (5′-TAATACGACTCACTATAGGG-3′ (forward); 5′-GCTAGTTATTGCTCAGCGG-3′ (reverse)) to give PCR gene product bioseq-ΔCys-E17C-N37C-DHFR. The amplified PCR product was then digested with BamHI and NdeI restriction enzymes, and the digested product was ligated into BamHI- and NdeI-cleaved bioseq-pET27b vector. A DHFR construct with a cysteine only at amino acid position 37 and biotinylation signal sequence at the N-terminus was prepared using the same primers and protocols from the pET27b plasmid for the wild-type DHFR. The sequences of these constructs were verified by DNA sequencing.

E. coli BL21(DE3) cells containing the new plasmid were grown at 37 °C in LB medium containing 50 mg/mL kanamycin to an absorbance of 0.6−0.7 at 600 nm and then induced at 37 °C for 5 h with 0.4 mM isopropyl-β-D-galactopyranoside. The enzyme was purified as previously described (*17*). Thirty milligrams of purified bioseq-ΔCys-E17C-N37C-DHFR was enzymatically biotinylated in vitro at room temperature for 24 h in 50 mM sodium phosphate, pH 7.2, containing 1 mM dithiothreitol, 4 mM biotin, 5 mM ATP, and 0.5 mg of biotin ligase to give biotin-ΔCys-E17C-N37C-DHFR (*18*). The reaction mixture was dialyzed to remove free biotin, ATP, and dithiothreitol, and the extent of biotinylation was determined (*19*). The extent of biotinylation was 80−90%, which is sufficient, since the biotinylated and unbiotinylated enzyme have the same catalytic activities and enzyme without biotin will not bind to the slide used for single-molecule experiments.

Preparation of Labeled DHFR. Biotin-ΔCys-E17C-N37C-DHFR (∼30 mg) was dissolved at 50 μM in deoxygenated 50 mM sodium phosphate, pH 7.2, at room temperature. A 10-fold molar excess of tris(2-carboxyethyl)phosphine was added to ensure that the cysteines were fully reduced. A 1 mM stock solution of Alexa555 (Molecular Probes) was prepared in water, and 0.5 molar equivalent of Alexa555 maleimide was added dropwise, with stirring, for each mole of protein. The reaction mixture (under argon) was protected from light by aluminum foil. The reaction was allowed to proceed for 2 h at room temperature; then another 0.5 molar equivalent of Alexa555 maleimide was added, and the reaction was allowed to proceed for 2 h. After a third addition of dye (0.5 molar equivalent), the reaction was allowed to proceed for ∼15−20 h. Free dye was removed by Sephadex G-25 column filtration followed by extensive dialysis at 4 °C against 50 mM sodium phosphate, pH 7.2. The protein solution was concentrated to ∼1 mM and filtered to remove any precipitated protein.

The final preparation, containing unlabeled, singly labeled, and double-labeled DHFR, was subjected to ion exchange chromatography on a prepacked Mono Q column with 1 mL bed volume. The protein with a single Alexa555 label has one additional negative charge, and the double-labeled enzyme has two additional negative charges. Separation was performed with a NaCl gradient (0.25−0.60 M) in 20 mM bis-trispropane and 1 mM dithiothreitol, pH 9.0, at a flow rate of 1 mL/min. The molecular masses of each fraction were determined by time-of-flight mass spectrometry with electrospray (+) ionization. The mass of unlabeled DHFR construct was determined to be 19 867 Da (calculated mass = 19 999 Da). Covalent attachment of one Alexa555 molecule to the unlabeled construct generated an additional mass of 956 Da, and addition of two Alexa555 molecules resulted in additional mass of 1910 Da. The fractions containing the singly labeled construct were then concen-

trated and extensively dialyzed against 50 mM sodium phosphate, pH 7.2. After dialysis, the DHFR was dissolved in deoxygenated 50 mM sodium phosphate, pH 7.2, to a final concentration of 1−3 μM. A 10-fold molar excess of tris-(2-carboxyethyl)phosphine was added to reduce possible disulfide bonds, and the solution was protected from light by aluminum foil.

The second label was put on the enzyme by adding 20 molar equivalents of 1 mM QSY35 iodoacetamide (Molecular Probes) in dimethyl sulfoxide to the enzyme (~1 μM), again dropwise with stirring. The reaction was allowed to proceed overnight at room temperature, covered from light. Free dye was removed by Sephadex G-25 column chromatography, followed by extensive dialysis at 4 °C against 50 mM sodium phosphate, pH 7.2. The final product was subjected to DHFR purification protocols involving methotrexate affinity chromatography to remove any misfolded protein molecules, with the exception that the folic acid concentration in the methotrexate affinity elution buffer was increased by 4-fold (*17*). Purified double-labeled DHFR (DHFR-Alexa555-QSY35) was concentrated and dialyzed against 50 mM sodium phosphate, pH 7.0, containing 10% glycerol. Aliquots were frozen in liquid N_2 and stored at −80 °C until use.

The final preparation is expected to contain enzyme with QSY35 and Alexa555 at amino acid positions 17 and 37, respectively, and the reverse labeling. The identity of the final product was confirmed by determining its mass by time-of-flight mass spectrometry with electrospray (+) ionization. The mass of double-labeled, biotinylated DHFR construct was determined to be approximately 21 390 Da. Covalent attachment of one QSY35 molecule to the construct generated an additional mass of 342, and biotinylation added 225 Da. The reactivities of the two cysteines were checked by preparing mutant enzymes with cysteine either at amino acid position 17 or 37. The kinetics of the reaction of these two species with Ellman reagent [5,5′-dithiobis-2-nitrobenzoic acid] were determined in a stopped-flow apparatus at pH 7.2 (50 mM sodium phosphate) by following the change in absorbance at 440 nm. Approximately 12 μM enzyme was reacted with 0.5−2.0 mM reagent. The second-order rate constants were found to be 115 $(mM)^{-1}$ s^{-1} and 88 $(mM)^{-1}$ s^{-1} for Cys 17 and Cys 37, respectively, indicating nearly equal reactivity.

A double-labeled DHFR was also prepared with the mutation G121V because this mutation, far from the catalytic site (Figure 1), has significant effects on the catalytic activity (*4*). The mutant construct (G121V-DHFR-Alexa555-QSY35) was prepared using similar protocols as the DHFR-Alexa555-QSY35 construct with the following exception. Two peaks of singly labeled G121V-DHFR-Alexa555 (same molecular weight by mass spectrometry) were obtained during separation of differently labeled species by anion exchange chromatography, and only the product that eluted first was used for the reported experiments.

Ensemble Kinetic Measurements. The steady-state turnover numbers (k_{cat}) for both forward and reverse reactions catalyzed by the DHFR-Alexa555-QSY35 construct were determined over the pH range 5−10 (*2*). Stopped-flow kinetics monitoring the absorbance at 340 nm (NADPH absorbance maximum) were used to determine the rate of the hydride transfer chemical step for the forward and reverse reaction at selected pH values (*2*). All ensemble kinetic measurements were carried out at 25 °C in 50 mM 2-morpholinoethane sulfonic acid, 25 mM tris(hydroxymethyl)-aminomethane, 25 mM ethanolamine, 100 mM NaCl, and 1 mM dithiothreitol. The concurrent conformational changes were explored by following the changes in Alexa555 fluorescence during the hydride transfer reaction with a stopped-flow apparatus (514 nm excitation, 550 nm bandpass filter emission). To study the forward reaction, the labeled DHFR (0.1−0.5 μM) was preincubated with NADPH (200 μM) prior to mixing with dihydrofolate to remove hysteretic behavior, and the reaction was initiated by mixing with an equal volume of dihydrofolate (200 μM). The reverse reaction was examined by preincubation of the labeled DHFR (0.5 μM) with 2 mM $NADP^+$ prior to mixing with an equal volume of 0.2 μM tetrahydrofolate. The solutions were degassed with argon to prevent oxidation of tetrahydrofolate.

Attachment of DHFR to the Surface of the Glass Slide. DHFR was attached to the surface of a glass cover slip by the following procedure. The cover slip was first washed extensively with methanol, 1 M NaOH, and 3 M HCl. It was then reacted with 0.2% 3-aminopropyltrimethoxysilane (United Chemical Technologies) in hexane for 30 min. This process resulted in a cover slip surface with exposed amino groups. The silanized cover slip was attached to a cleaned glass microscope slide after putting two triple layers of double-sided Scotch tape on the edges of the slide to hold the cover slip in place. An approximate 10 mM solution of 6-((biotinoyl)amino)hexanoic acid, succinimidyl ester (Molecular Probes) was prepared by first dissolving the solid reagent in 100 μL of dimethyl sulfoxide and then bringing the solution to a total volume of 1 mL using 100 mM sodium phosphate, pH 9. The biotin-succinimide ester (100 μL) was then passed between the slide and cover slip using capillary action. The biotinylation reaction was allowed to proceed for 1.5 h with fresh biotin (100 μL) being added every 30 min. After 1.5 h, the liquid between the slide and cover slip was replaced with 100 mM sodium phosphate and 100 mM NaCl, pH 7.0, supplemented with 15 μM bovine serum albumin. NeutrAvidin (100 nM) (Molecular Probes) was added to the slide using capillary action and allowed to react for 30 min. Nonreacted NeutrAvidin was removed by passing 500 μL of buffer between the slide and the cover slip using capillary action. One hundred microliters of double-labeled DHFR (100 nM) was then added and allowed to react for 10 min. This process was repeated three times. Unbound DHFR was removed by three washes with buffer solution. A substrate mixture (12 μM DHF, 20 μM NADPH or NADPD, 2 mM $NADP^+$, 100 mM sodium phosphate, 100 mM NaCl, pH 8.5, and 15 μM bovine serum albumin) was then added and allowed to react for 1 h prior to viewing with a Zeiss inverted microscope. The equilibrium mixture of substrates and pH 8.5 were used to maximize the concentration of enzyme−substrate intermediates. Similar experiments were carried out at pH 7.5. Experiments were also carried out with DHFR with only 10 μM DHF, 20 μM NADPH, or 2 mM $NADP^+$ present.

The enzymatic activity of the enzyme attached to the slide was measured by following the decrease in absorbance of NADPH at pH 8.5. The calculated turnover number is 1−11 s^{-1} assuming the surface-bound DHFR has an effective concentration of 10−1 nM, respectively. The turnover

number in solution is 6 s^{-1} so that the surface-bound enzyme has essentially full catalytic activity.

Time Course Analysis of Single Molecules of DHFR. Fields of well-dispersed single molecules were first identified using a Zeiss inverted microscope equipped with a Pentamax ICCD camera (Roper Scientific) and Ar laser. Time courses (trajectories) of single DHFR molecules were then followed with an avalanche photodiode (SPCM-AQR-16, Perkin-Elmer) with photons counted in 500 μs increments. The slide was moved via computer control to a position where a single molecule was located (maximum in fluorescence intensity), and the trajectory of the fluorescence was then measured. Lifetimes were collected for the high and low fluorescent states, with the two states defined by drawing a line through the center of the fluctuations. The lifetimes for individual DHFR molecules were tabulated for a minimum of 400 events and plotted to give the distribution for the number of events occurring for each range of lifetimes.

RESULTS

Kinetic Characterization of Double-Labeled Enzyme. The steady-state turnover numbers (k_{cat}) of the double-labeled enzyme for the forward and reverse reactions are very similar to the wild-type enzyme over the pH range 5−10. The pH-independent value of k_{cat} for the forward direction is 11.4 s^{-1}, and the single pK_a characterizing the pH dependence is 8.4, versus 12.5 s^{-1} and 8.5 for the wild-type enzyme (*2*, *17*). The corresponding values for the reverse reaction are 0.6 s^{-1} and 8.0 versus 0.6 s^{-1} and 7.8 for wild-type enzyme. Thus, the steady-state properties of the construct are very similar to those of the wild-type enzyme.

The hydride transfer rate constant was determined from the burst of the absorbance decrease at 340 nm in the stopped-flow apparatus. At pH 7.0, the rate constant is 210 s^{-1} versus 228 s^{-1} for wild-type enzyme, and the magnitude of the burst corresponds to enzyme concentration. At pH 7.5, the hydride transfer rate constant is 86 s^{-1}, and at pH 8.5, it is 9.4 s^{-1}. Above pH 8.5, the hydride transfer rate is the same as the turnover number, and for the reverse reaction, the hydride transfer rate constant is equal to the turnover number for the pH range studied (*2, 17*).

Ensemble FRET Measurements. Stopped-flow measurements of the change in fluorescence of Alexa555 indicated an increase in fluorescence occurred when the reaction was initiated, as shown in Figure 2. The change in fluorescence was only observed when the substrate, DHF, was present, ruling out the possibility that the increase was caused by dilution of labeled enzyme. The increase in Alexa555 emission was not observed for the singly labeled DHFR constructs, DHFR-Alexa555 (at residue 17) and DHFR-Alexa555 (at residue 37), suggesting that the observed signal is due to energy transfer between Alexa555 donor and QSY35 quencher and not solely to changes in probe environment. The increase in fluorescence in the forward direction is approximately 5%, whereas in the reverse direction, it is 1.5%. The first-order rate constants for the change in fluorescence are summarized in Table 1. The rate of Alexa555 emission increase was found not to depend on substrate (DHF) concentration, indicating that an intramolecular reaction is being observed. Furthermore, an identical change in fluorescence and similar associated first-order rate

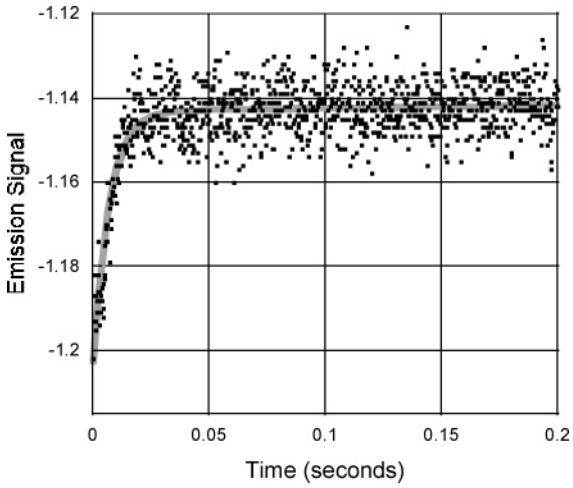

FIGURE 2: Stopped-flow time course for the reaction of the double-labeled DHFR with 100 μM NADPH and 100 μM dihydrofolate at pH 8.5. Excitation at 514 nm; 550 nm cutoff filter for emission. The data (black dots) are fit to a single-exponential (line) with a rate constant of 211 s^{-1}.

Table 1: First Order Rate Constants for the Stopped-Flow Fluorescence Change[a]

pH	forward reaction k (s^{-1})	reverse reaction k (s^{-1})
6.0	254	–
7.0	282 (154)	–
7.5	170	30
8.5	211 (92)	31
10.0	153	42

[a] Both 0.5 μM double-labeled DHFR and 200 μM NADPH were mixed with 200 μM DHF for the forward reaction, and 0.5 μM double-labeled DHFR and 2 mM $NADP^+$ were mixed with 200 μM tetrahydrofolate for the reverse reaction. The results for the double-labeled G121V mutant are given in parentheses.

constant were obtained for the forward direction even in the absence of NADPH (pH 7.0). For the forward direction, the rate constant was also determined with NADPD as substrate. No measurable isotope effect was observed. Rate constants for the G121V-Alexa555-QSY35 DHFR for the forward reaction at pH 7.0 and 8.5 are included in Table 1. The estimated error in the rate constants is ±15%.

Single-Molecule Measurements. Fields of well-resolved single molecules of DHFR were observed as previously demonstrated (*3*). No significant time dependence of the fluorescence intensity was observed in the absence of substrates (Figure 3A), but the fluorescence of single molecules fluctuated when an equilibrium mixture of substrates was present (Figure 3B). In addition to the dependence on the presence of an equilibrium mixture of substrates, the observed fluctuation was unchanged over a range of laser intensities, so it is unlikely to be a photochemical reaction. In the presence of substrates, two populations of molecules were observed, one with a relatively high fluorescence and one with a significantly lower fluorescence (~50%). These two populations are attributed to the two possible arrangements of the spectroscopic probes: E17C-QSY35, N37C-Alexa555 and E17C-Alexa555, N37C-QSY35. Since E18C-Alexa488 is significantly quenched when substrates bind (*3*), the low-fluorescence species was attributed to the latter arrangement. Only the high-fluorescence species was studied

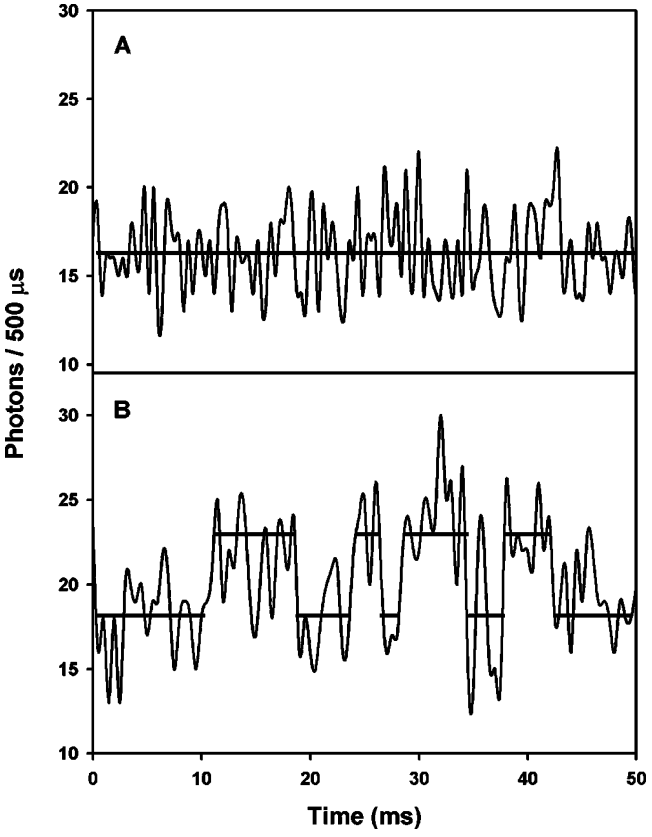

FIGURE 3: (A) Fluorescence emission intensity (photons/500 μs) versus time for a single molecule of the double-labeled DHFR in the absence of substrates at pH 8.5, 100 mM sodium phosphate, 100 mM NaCl, and 15 μM bovine serum albumin. (B) Same as panel A after incubation with 12 μM dihydrofolate, 20 μM NADPH, and 2 mM $NADP^+$. The horizontal lines indicate the scoring of an event with lifetime τ.

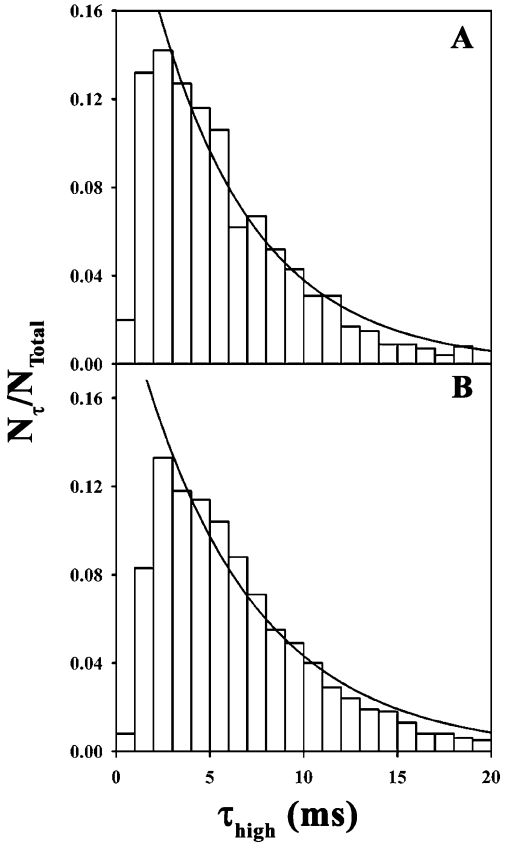

FIGURE 4: Plot of the probability distributions of the reaction lifetimes τ, N_τ/N_{total}, for the high-fluorescence state versus τ from trajectories measured at pH 8.5. (Initial reaction mixture: 12 μM dihydrofolate, 20 μM NADPH or NADPD, and 2 mM $NADP^+$ in 100 mM sodium phosphate, 100 mM NaCl, and 15 μM bovine serum albumin.) The solid line is the weighted nonlinear least-squares fit to eq 2, neglecting reaction lifetimes shorter than 2 ms. (A) NADPH; (B) NADPD.

in detail. Fluctuations of fluorescence intensity were observed only with an equilibrium mixture of substrates and not with the individual substrates DHF, NADPH, or $NADP^+$.

Plots of the probability of the occurrence of a lifetime (τ) versus the lifetime are shown in Figures 4 and 5 for both the high- and low-fluorescence states, and for both NADPH and NADPD as substrates. More than 1200 lifetimes were measured for each state. The distributions were essentially the same for individual spots and for samples analyzed on different days. Thus, this behavior is characteristic of all of the single molecules, with the proviso above with regard to the two possible orientations of the probes.

In addition to the determination of the reaction lifetimes, the trajectories were analyzed by plotting the frequency of the number of photons versus the number of photons (*20*). Representative results are displayed in Figure 6 for trajectories in the absence of substrates and in the presence of an equilibrium mixture of substrates. In the absence of substrates (panel A), a symmetrical curve is obtained, whereas in the presence of substrates, a bimodal distribution can be seen (panel B). This is consistent with the existence of two fluorescent states in the presence of substrates and one state in their absence. Over 100 trajectories of 100 ms or longer were examined, and the characteristic double peaks were found in all but a few cases. The few exceptions were primarily trajectories in which the number of photon counts was very low ($<$10 photons/500 μs), thereby limiting the resolution of the analysis. In many cases, the width of the photon distribution is similar in both the presence and absence of substrates. This suggests that in the absence of substrate, conformational transitions may be occurring that are faster than the time resolution of the equipment.

For a one-step unimolecular reaction, the distribution of lifetimes is described by a single-exponential function from which the ensemble average rate constant can be obtained (*21*). The observed lifetime distributions are not consistent with this behavior, but the undercounting of events for short lifetimes often is observed (cf. *22*). A mechanism formally consistent with the data is

$$A \xrightarrow{k_1} B \xrightarrow{k_2} C \qquad (1)$$

However, this mechanism assumes a unidirectional flux, which is not possible for a reversible system at equilibrium. This was confirmed by simulations of lifetime distributions for reversible mechanisms. We conclude, consequently, that the number of events for short lifetimes has been undercounted due to limitations in the time resolution of the experiment. In light of these considerations, the data have been analyzed in terms of a unimolecular one-step reaction with an ensemble rate constant k, neglecting reaction lifetimes less than 2 ms. For this reaction, the distribution of lifetimes is given by the relationship

$$N_\tau/N_{total} = k \exp(-k\tau) \qquad (2)$$

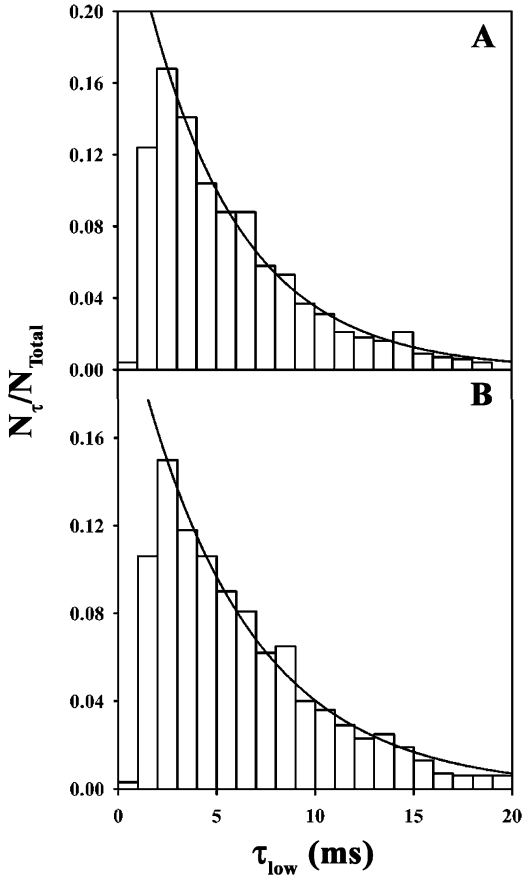

FIGURE 5: Plot of the probability distributions of the reaction lifetimes τ, N_τ/N_{total}, for the low-fluorescence state versus τ from trajectories measured at pH 8.5. (Initial reaction mixture: 12 μM dihydrofolate, 20 μM NADPH or NADPD, and 2 mM $NADP^+$ in 100 mM sodium phosphate, 100 mM NaCl, and 15 μM bovine serum albumin.) The solid line is the weighted nonlinear least-squares fit to eq 2, neglecting reaction lifetimes shorter than 2 ms. (A) NADPH; (B) NADPD.

where N_τ is the number of events with a lifetime τ, and N_{total} is the total number of events.

A nonlinear weighted least-squares fit of the data to eq 2 is included in Figures 4 and 5, and the associated rate constants for the four probability distributions are summarized in Table 2. [The weighting used was (1/standard deviation)^2]. The uncertainty in the rate constants is estimated as $\pm$15%. Within the experimental uncertainty, no isotope effect is seen for any of the rate constants (NADPH versus NADPD). Included in Table 2 are the rate constants characterizing the reaction lifetime probability distribution at pH 7.5. At this pH, each probability distribution was based on more than 400 lifetimes for each fluorescent state. Also included in Table 2 are the rate constants for the G121V-double-labeled DHFR at pH 8.5 with NADPH as the substrate.

Distance Changes Associated with Observed Reactions. The dependence of fluorescence energy transfer on the distance between the two probes is given by

$$\frac{F_\infty - F}{F_\infty} = \frac{1}{1 + (R/R_0)^6} \tag{3}$$

where F_∞ is the fluorescence of the donor at infinite distance, F is the observed fluorescence, R is the distance between probes, and R_0 is the distance at which 50% energy transfer occurs. For the two probes used, $R_0 = 24$ Å, and the X-ray structure of DHFR suggests that $R \sim 28$ Å.

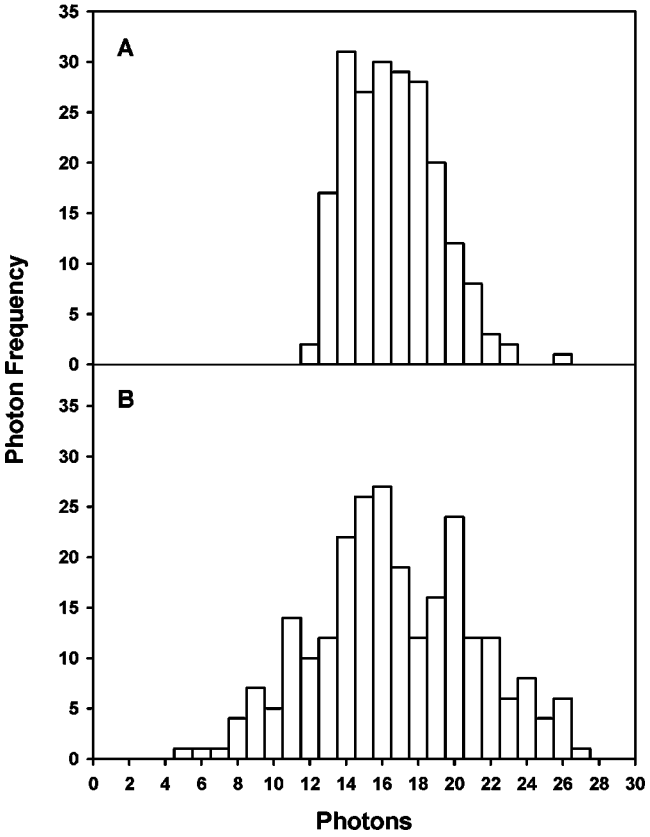

FIGURE 6: Plot of the frequency of the number of photons observed versus the number of photons for a 200 ms trajectory. (A) Double-labeled DHFR in the absence of substrates at pH 8.5, 100 mM sodium phosphate, 100 mM NaCl, and 15 μM bovine serum albumin. (B) Same as panel A after incubation with 12 μM dihydrofolate, 20 μM NADPH, and 2 mM $NADP^+$.

Table 2: Ensemble Average Rate Constants Determined from Single-Molecule Lifetime Distributions[a]

pH	fluorescent state	substrate	k (s^{-1})
8.5	high	NADPH	185
8.5	low	NADPH	210
8.5	high	NADPD	170
8.5	low	NADPD	170
8.5[b]	high	NADPH	160
8.5[b]	low	NADPH	145
7.5	high	NADPH	155
7.5	low	NADPH	150
7.5	high	NADPD	165
7.5	low	NADPD	130

[a] Double-labeled DHFR. Initial substrate concentrations: 12 μM dihydrofolate, 2 mM $NADP^+$, and 20 μM NADPH or NADPD in 100 mM sodium phosphate, 100 mM NaCl, and 15 μM bovine serum albumin. [b] G121V double-labeled DHFR.

The total differential of eq 3 with F and R as variables is

$$\frac{\Delta F}{F_\infty - F} = \frac{6(\Delta R/R)}{1 + (R_0/R)^6} \tag{4}$$

The total distance change was determined from the change in fluorescence intensity relative to the calculated intensity at $R = \infty$. From eq 4, the total distance change between the

two probes in changing fluorescence states is estimated to be 1−2 Å for the single-molecule experiments.

In principle, the fluorescence changes observed can be due to factors other than a change in distance between the probes. However, the Alexa555 is attached to an external amino acid not near the active site and has considerable rotational freedom, as judged by the anisotropy (0.25 in the absence of substrates; 0.24 in the equilibrium mixture of substrates used in the single-molecule experiments, pH 8.5), and the rotational freedom is not significantly altered by the presence of substrates. Unrestricted or somewhat restricted molecular rotations are typically associated with time constants on the nanosecond time scale. We did not observe an increase in the Alexa555 emission for singly labeled DHFR constructs labeled at either residue 17 or 37, also suggesting that the changes in emission are not due to environmental effects. Also since $R \sim R_0$, changes in fluorescence due to FRET are maximized. Thus, it seems most likely that the fluorescence change is primarily due to a change in distance between the acceptor and donor so that the calculated distances represent a semiquantitative measure of the extent of the conformational change.

DISCUSSION

The results obtained from stopped-flow experiments suggest that the FRET pair on DHFR is detecting a conformational change prior to hydride transfer in the forward direction (dihydrofolate + NADPH). The increase in Alexa555 emission indicates that residues 17 and 37 are moving further away from each other during the reaction being observed. The ensemble rate constants obtained from the stopped-flow and single-molecule experiments are similar, about 200 s^{-1} at pH 8.5. However, the conformational changes observed for the two types of experiments may not be identical. In the case of ensemble experiments, a conformational change is observed en route to a final equilibrium mixture, whereas a conformational change is observed with an equilibrium mixture of substrates for the single-molecule experiments. Consequently, a transient conformation could be observed in the ensemble experiments that may not be present in the equilibrium mixture used in the single-molecule experiments. This possibility is supported by the finding that a conformational change was detected after mixing DHFR with DHF in the ensemble experiments but not in the equilibrium mixture of DHF and DHFR in single-molecule experiments. Thus, in the case of stopped-flow experiments, the conformational change precedes hydride transfer, whereas in the case of the single-molecule experiments, it could be either before or after hydride transfer.

The pH dependence of the rate constants in Tables 1 and 2 is not very large, falling almost within the experimental uncertainties. Neither the single-molecule nor the stopped-flow ensemble rate constants have an observable isotope rate effect so that hydride transfer is not directly linked to the FRET changes. Previous single-molecule experiments have reported an isotope effect using Alexa488 quenching at the catalytic site as an observable (*3*), but this is not seen in the present system.

The ensemble rate constants (Table 1) for the G121V mutant are significantly reduced, and the corresponding rate constants obtained from the single-molecule experiments also are reduced, although the reduction is close to the maximum experimental uncertainties. These results suggest that the conformational change may be associated with the enzymatic mechanism. Previously, pre-steady-state kinetic analysis of tryptophan fluorescence of the G121V mutant revealed a conformational change which preceded chemistry that occurred with a first-order rate constant of 3.5 s^{-1} (*4*). Thus, at least two different conformational changes for the G121V mutant take place at different rates and are likely to precede hydride transfer. These multiple conformational fluctuations may be crucial for preparing the enzyme for the hydride transfer step. The ensemble rate constants for the reverse direction (Table 1) are much less than those associated with the forward reaction but greater than associated with hydride transfer. This suggests a conformational change precedes the hydride transfer step for the reverse reaction.

Although the calculation of the distance change associated with the conformational change is subject to the caveats discussed above, 1−2 Å is probably a reasonable estimate. Theoretical calculations have suggested that distance changes of individual residues in the 1 Å range are associated with the hydride transfer reaction (*14*). Both of these results are consistent with the idea that very small conformational changes are involved in the modulation of enzyme catalysis. Furthermore, the decrease in rate constants observed for the G121V mutant is consistent with the concept that the catalytic process involves coordination of the entire enzyme structure, not just the structure immediately adjacent to the active site.

DHFR is known to have multiple conformations, even in the absence of substrates, and large changes in distances, of the order of 10 Å, have been proposed as part of the catalytic mechanism from X-ray crystallography studies. However, it is not clear whether these changes are part of the intimate catalytic process or represent going from an essentially inactive form of the enzyme to an active form. Recent NMR studies have suggested loop motions both prior to and after hydride transfer, with the former having rate constants in the range of $10-10^2$ s^{-1} and the latter greater than 10^3 s^{-1} (*23*).

It is instructive to consider a possible model for enzyme catalysis that incorporates the multiple conformations that have been observed, the differences in conformational changes sometimes found with different methods (e.g., stopped-flow and single molecule), and the dynamic heterogeneity encountered in some single-molecule experiments (cf. *21*). A protein can be viewed as existing in multiple conformations that interconvert, a view routinely utilized in the field of protein folding (cf. *24*). When the enzyme−substrate complex forms, it can be viewed as multiple interconverting conformations. Some of these conformations are capable of catalysis, although the rate of catalysis associated with each catalytically competent conformation may be different. Thus, in writing the reaction sequence, each of the members of the family of conformations present in the initial enzyme−substrate complex formed goes through

a series of conformational changes leading to catalysis. This can be written schematically as

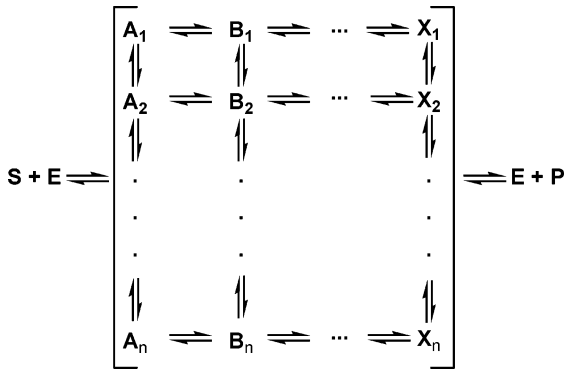

For simplicity, the multiple conformations of E are not shown, and only a single substrate, S, and product, P, are shown. In this schematic equation, the A_i, B_i, C_i, and so forth, represent conformations of enzyme−substrate complexes that are in the catalytic pathway, and parallel catalytic pathways exist, $A_1 \rightarrow B_1 \rightarrow ... \rightarrow X_1$, and so forth.

If the A_i conformations, B_i conformations, and so forth, are in rapid equilibrium relative to the rates of interconversion of reaction intermediates, then the reaction will appear to proceed as a single reaction represented as $\sum A_i \rightarrow \sum B_i \rightarrow ... \rightarrow \sum X_i$, and only the average conformation of each reaction intermediate is observed experimentally. At the other limit, if the A_i conformations, B_i conformations, and so forth, equilibrate slowly relative to the rates of interconversion of intermediates along the catalytic pathway, catalysis will occur through independent catalytic paths. In other words, each conformation will act as an independent enzyme. At the single-molecule level, each molecule could have a different catalytic rate constant and a different FRET for pairs of probes. This would be seen as apparent static heterogeneity, that is, preexisting multiple conformations that are catalytically competent. At the ensemble level, the observed catalytic rate would be obtained by adding the reciprocal of the flux for each pathway, and it would be exceedingly difficult to distinguish between the pathways. (Calculation of the flux requires knowledge of both the rate constants and the concentrations of intermediates.) The intermediate case, when the rates of interconversion of the A_i conformations, B_i conformations, and so forth, are comparable to the rates of interconversion of intermediates along the catalytic pathway, also is a distinct possibility. In this case, the population of conformations present before adding substrate could be different than the equilibrium population of conformations present at equilibrium in the presence of both substrates. This could cause different results to be seen with the stopped-flow and equilibrium experiments. On the single-molecule level, this would appear as dynamic heterogeneity, that is, differences in catalytic rates for different molecules (*21*). This model also allows for different degrees of cooperativity in the conformational changes, depending on which pathways dominate, and for different effects of chemical labels, that is, fluorescent labels and FRET.

In terms of this model, the conformational changes observed in this work appear to be of some significance for catalysis based on the results obtained with the G121V mutant but are probably not closely coupled to the hydride transfer step. This is suggested by the fact that the hydride transfer rate constant is reduced 170-fold (at pH 7.0) in the mutated enzyme, whereas the rate constants associated with the measured conformational change are reduced only by 2-fold (ensemble) or less (single molecule). Also the rate constants for the conformational change do not have isotope rate effects, although we would not necessarily expect an isotope effect for a conformational change coupled to the hydride transfer step assuming that the role of this conformational change was, for example, to preorganize the active site. At low pH (<5.0), the values for the hydride transfer rate constants for wild-type DHFR are about 950 s^{-1} in the forward direction and 0.02 s^{-1} in the reverse direction. The hydride transfer rates vary with pH to 0.3 s^{-1} and 0.6 s^{-1} at pH 10 for the forward and reverse direction, respectively. In contrast, the rate constants for the observed conformational changes do not appear to depend greatly on pH. Thus, at low pH values, the conformational changes observed are unlikely to be on the dominant catalytic pathway for the forward reaction because slow conformational changes preceding the hydride transfer step would probably have been revealed by pre-steady-state kinetic measurements. With the proposed model, conformations and pathways can be shifted as the pH varies. This said, the rates of conformational changes may not necessarily vary with pH if the dynamical fluctuations do not depend on the protonation state of the enzyme in a manner similar to the hydride transfer rate. The conformational changes observed might not be on the primary catalytic pathway and/or they could be organizational steps prior to hydride transfer not greatly affected by mutation.

Although this model appears complex, it is really quite simple conceptually and may be useful for understanding the role of multiple conformational changes in catalysis. It also may be useful for understanding the relationships between ensemble measurements and single-molecule measurements. A more complex model can be envisaged that permits the interconversion of more species, for example, $A_1 \rightarrow B_2$, but this is not conceptually different. The crux is that the existence of coupled multiple conformations and catalytic pathways permits different conformational modes to be of importance, depending on the external conditions and protein modifications. Moreover, catalysis can be pictured as occurring simultaneously through closely related multiple pathways and conformations.

As discussed above, neither isotope effects nor pH dependence is necessarily expected for a conformational motion that is closely coupled to catalysis. Moreover, it is also not clear what rates would be expected for conformational motions correlated with hydride transfer, although a close correspondence between the rate of a given conformational change and that of hydride transfer seems to be a necessary condition. To gain insight into the possible connection between a particular motion and catalysis, DHFR variants with decreased hydride transfer rates and/or altered rates for other steps in the catalytic cycle will be examined via FRET pairs attached to various locations in DHFR. The finding of a commensurate, altered conformational change rate for a mutant DHFR with altered catalytic rates would unequivocally indicate that the FRET pair is detecting a motion some part of which lies along the reaction coordinate. The opposite is not true, as the rate of a motion may be

unaffected by a mutation influencing the hydride transfer rate, for example, if the motion plays a role in preorganizing the active site for hydride transfer and this preorganization step is not affected in the mutant.

ACKNOWLEDGMENT

We are indebted to Professor Rick Russell, University of Texas, for carrying out the single-molecule lifetime simulations.

REFERENCES

1. Sawaya, M. R., and Kraut, J. (1997) Loop and subdomain movements in the mechanism of *Escherichia coli* dihydrofolate reductase: crystallographic evidence, *Biochemistry 36*, 586−603.
2. Fierke, C. A., Johnson, K. A., and Benkovic, S. J. (1987) Construction and evaluation of the kinetic scheme associated with dihydrofolate reductase from *Escherichia coli*, *Biochemistry 26*, 4085−4092.
3. Zhang, Z., Rajagopalan, P. T. R., Selzer, T., Benkovic, S. J., and Hammes, G. G. (2004) Single-molecule and transient kinetics investigation of the interaction of dihydrofolate reductase with NADPH and dihydrofolate, *Proc. Natl. Acad. Sci. U.S.A. 101*, 2764−2769.
4. Cameron, C., and Benkovic, S. J. (1997) Evidence for a functional role of the dynamics of glycine-121 of *Escherichia coli* dihydrofolate reductase obtained from kinetic analysis of a site-directed mutant, *Biochemistry 36*, 15792−15800.
5. Penner, M. H., and Frieden, C. (1987) Kinetic analysis of the mechanism of *Escherichia coli* dihydrofolate reductase, *J. Biol. Chem. 262*, 15908−15914.
6. Stone, S. R., and Morrison, J. F. (1982) Kinetic mechanism of the reaction catalyzed by dihydrofolate reductase from *Escherichia coli*, *Biochemistry 21*, 3757−3765.
7. Lumry, R. (1959) Some aspects of the thermodynamics and mechanism of enzymic catalysis, in *The Enzymes* (Boyer, P., Ed.) 2nd ed., Vol. 1, p 157−231, Academic Press, New York.
8. Koshland, D. E., Jr. (1960) The active site and enzyme action, *Adv. Enzymol. 22*, 45−97.
9. Hammes, G. G. (1964) Mechanism of enzyme catalysis, *Nature 204*, 342−343.
10. Hammes, G. G. (1982) *Enzyme Catalysis and Regulation*, pp 99−109, Academic Press, New York.
11. Hammes, G. G. (2002) Multiple conformational changes in enzyme catalysis, *Biochemistry 26*, 8221−8228.
12. Benkovic, S. J., and Hammes-Schiffer, S. (2003) A perspective on enzyme catalysis, *Science 301*, 1196−1202.
13. Epstein, D. M., Benkovic, S. J., and Wright, P. E. (1995) Dynamics of the dihydrofolate reductase-folate complex: catalytic sites and regions known to undergo conformational change exhibit diverse dynamical features, *Biochemistry 34*, 11037−11048.
14. Agarwal, P. K., Billeter, S. R., Rajagopalan, P. T. R., Benkovic, S. J., and Hammes-Schiffer, S. (2002) Network of coupled promoting motions in enzyme catalysis, *Proc. Natl. Acad. Sci. U.S.A. 99*, 2794−2799.
15. Bystroff, C., and Kraut, J. (1990) Crystal structure of unliganded *Escherichia coli* dihydrofolate reductase ligand-induced conformational changes and cooperativity in binding, *Biochemistry 30*, 2227−2239.
16. Rajagopalan, P. T., Zhang, Z., McCourt, L., Dwyer, M., Benkovic, S. J., and Hammes, G. G. (2002) Interaction of dihydrofolate reductase with methotrexate: ensemble and single-molecule kinetics, *Proc. Natl. Acad. Sci. U.S.A.* 99, 13481−13486.
17. Miller, G. P., Wahnon, D. C., and Benkovic, S. J. (2001) Interloop contacts modulate ligand cycling during catalysis by *Escherichia coli* dihydrofolate reductase, *Biochemistry. 40*, 867−875.
18. Beckett, D., Kovaleva, E., and Schatz, P. J. (1999) A minimal peptide substrate in biotin holoenzyme synthetase-catalyzed biotinylation, *Protein Sci. 8*, *921*−*929*.
19. Janolino, V. G., Fontecha, J., and Swaisgood, H. E. (1996) A spectrophotometricassay for biotin-binding sites of immobilized avidin, *Appl. Biochem. Biotechnol. 56*, 1−7.
20. Chen, Y., Müller, J. D., So, P. T. C., and Gratton, E. (1999) The photon counting histogram in fluorescence fluctuation spectroscopy, *Biophys. J. 77*, 553−567.
21. Lu, H. P., Xun, L., and Xie, X. S. (1998) Single molecule enzymatic dynamics, *Science 282*, 1877−1882.
22. Hohng, S., and Ha, T. (2005) Single molecule quantum-dot fluorescence resonance energy transfer, *ChemPhysChem 6*, 956−960.
23. McElheny, D. Schnell, J. R., Lansing, J. C., Dyson, H. J., and Wright, P. E. (2005) Defining the role of active-site loop fluctuations in dihydrofolate reductase catalysis, *Proc. Natl. Acad. Sci. U.S.A. 102*, 5032−5037.
24. Merlo, C., Dill, K. A., and Weikl, T. R. (2005) Φ values in protein-folding kinetics have energetic and structural components, *Proc. Natl. Acad. Sci. U.S.A. 102*, 10171−10175.

BI051378I